Modeling the Spread of *Phytophthora*

A. Henkel · J. Müller · C. Pötzsche

Abstract We consider a model for the morphology and growth of the fungus-like plant pathogen *Phytophthora* using the example of *Phytophthora plurivora*. Here, we are utilizing a correlated random walk describing the density of tips. This random walk incorporates a delay in branching behavior: newly split tips only start to grow after a short while.

First, we question the effect of such a delay on the running fronts, for uniform- as well as non-uniform turning kernels. We find that this delay primarily influences the slope of the front and therewith the way of spatial appropriation, and not its velocity. Our theoretical predictions are confirmed by the growth of *Phytophthora* in concrete experiments performed in Petri dishes. The second question addressed in this paper, concerns the manner tips are interacting, especially the point why tips stop to grow "behind" the interface of the front, respectively in confrontation experiments at the interface between two colonies. The combination of experimental data about the spatially structured time course of the glucose concentration and simulations of a model taking into account both, tips and glucose, reveals that nutrient depletion is most likely the central mechanism of tip interaction and hyphal growth inhibition. We presume that this is the growing mechanism for our kind of *Phytophthora* in infected plant tissue. Thus, the pathogen will sap its hosts via energy depletion and tissue destruction in infected areas.

A. Henkel (E-mail: annett_henkel@email.de)
Pathologie der Waldbäume, TU München, Hans-Carl-von-Carlowitz-Platz 2, 85354 Freising

J. Müller (E-mail: johannes.mueller@mytum.de)
C. Pötzsche (E-mail: poetzsch@ma.tum.de)
Zentrum Mathematik, TU München, Boltzmannstraße 3, 85758 Garching, Germany

1 Introduction

The genus *Phytophthora* de Bary, belonging to the Class Oomycetes, is a well-known group of fungus-like pathogens with algal relatives which are the causal agent for some of the most devastating plant diseases. Herbaceous crops like potatoes as well as woody crops like citrus or even trees in natural forests fall prey to them [10,19]. This leads to tremendous pecuniary and ecological losses each year, attracting a lot of interest in the investigation of the behaviour and spread of *Phytophthora* [20].

Nevertheless, doing research in phytopathology is an intricate work due to the complexity of interactions between host and pathogen. Hence, the scientific progress in working with *Phytophthora* has happened on different scales: the interaction between a molecular and cellular level e.g [4,39,41], on the whole plant level e.g. [3,6,11–14,34], or on the pathogenic impact on different species e.g. [12,24,40,43]. Furthermore, Cahill et al. [5] investigate the dimensions of the ecological impact of *P. cinnamomi* Rands in Australia and provide an application of management strategies. For all these interesting results the precise mechanism of killing a tree is not well understood.

The aim of the present paper is to investigate the growth of *Phytophthora* focussing on its morphology. In difference to most studies performed up to now, the complexity of the host-pathogen system is circumvented in constructing a more controlled setup: the pathogen is grown in a medium, simulating a host proving a certain nutrient supply. More complex feedback like induced reactions by the host are excluded. This is, we try to obtain an in depth understanding of the first step from the pathogen's point of view. The pathogen we are working at is *Phytophthora citricola* Sawada, which was recently revealed to be a new species named *Phytophthora plurivora* (cf. [23]). Indeed, Jung and Burgess [23] and citations therein also showed that this *Phytophthora* is causing progressive destruction of large portions of the root system. In addition, it is predisposing the trees to droughts and attacks by secondary pests and pathogens which results in an impairment of the host with lethal outcome.

The mathematical approaches encountered so far mostly focus on the overall spread of *Phytophthora*, using general model structures developed to describe the spread of infectious diseases. E.g. [31] investigates a model without spatial structure, in order to understand the effect of variability in the susceptibility of plants; also the controllability in models without spatial structure has been considered, see e.g. [2,15,30] and references therein. Spatial models were developed, again basically in order to investigate the controllability of *Phytophthora*, at a macroscopic level, see e.g. [21,37]. On the other hand, models for the gene network on a molecular level were investigated in [33].

The phenomenon we are considering in the present work describes the propagation on the microscopic and mesoscopic scale. Indeed, we model the spread of hyphae, the long filaments in which *Phytophthora* grows, and tips which represent the top of the filaments where actual growth takes place, see e.g. Fig. 1. We investigate the most striking mechanisms affecting this spread, and analyse the interaction between tips depending on carbohydrate supply

as essential alimental impulse. We suppose that the growth of the pathogen is regulated by offered carbohydrates whether in culture media or in the tissue of an host. That is the intention of a pathogen — getting alimental nutrients from the host.

The model structure we base on is the correlated random walk for tips, since a diffusion approximation is hardly appropriate: In fact, a diffusion approximation of the spread of entities relies on the assumption that particles rapidly "forget" their history [22], especially the direction they have been moving in. This means, in order to use diffusion, it is necessary that the particles often change direction in a relatively uncorrelated manner. For a general survey of random walk models in biology we refer to [7] or [32, 29].

In fact, the tips of *Phytophthora* tend to proceed to grow in the direction they did select, and a change in this direction is rare. Thus, a correlated random walk is a better model for *Phytophthora* than a diffusion equation. Fortunately, such kinds of models have been well investigated [17, 18, 22, 35]. In the present case, however, some non-standard ingredients are required to model the growth of *Phytophthora* in an appropriate way: Basically, new directions do not come in via the change of a direction by an existing tip, but tips split and the new tip selects a new direction, while the old tips continuous their straight growth. Thus, population growth and directional change are intertwined. A second special ingredient of our model represents the fact that the new tip does not start to grow at once but only after a small delay. Such a delay was already observed in 1924 at *Botrytis cinerea* Pers. [38] and discussed 1994 as apical dominance in Griffin [16].

Consequently, the first aim of the paper is to provide an appropriate model framework, and a basic idea about the effects caused by the delay. The second central question of our modeling approach is the interaction of tips, where data clearly show a front-like behavior.

Though we are not aware of other models that describe *Phytophthora* at the spatial scale addressed here, there is a vast amount of literature addressing fungal growth in general, or focussing on other fungae. There are many models for tips and hyphae, using discrete structures resembling stochastic cellular automata (see e.g. [42], and quotations herein), or based on partial differential equations (e.g. [8]). Most of these models carry a parabolic structure, either directly as they consist of parabolic partial differential equations, or as they are discrete but use a parabolic scaling (see e.g. the review article [9]). At the end of the day, these models assume a mixture of diffusion and directed growth of fungae. Meskauskas and coworkers [27] present an approach which does not incorporate a diffusive component. These ideas are close to the setup used in the present work. In their model, which is exclusively of algorithmic nature, tips grow guided and directed by a tropic field, and new directions arise via branching. In this way, they are able to produce a variety of morphological structures observed for different fungal species. In comparison, the model discussed in the present work is kept more simple to allow for analytic treatment of some key features, but complex enough to permit a quantitative, model-based analysis of experiments.

2 Model

We denote time by t, a point in the plane by $x = (x_1, x_2) \in \mathbb{R}^2$, and the velocity of a tip by $v = (v_1, v_2) \in \mathbb{R}^2$. In a given location and a given time, the absolute value γ of the velocity is assumed to be the same for all tips, i.e. $v \in \gamma\mathbb{S}^1$. We discuss the parameter γ below. Instead of the true velocity, we use a rescaled velocity in $\mathbb{S}^1$, which we denote again by v. This should not lead to confusion, as we only use this rescaled velocity $v \in V = \mathbb{S}^1$ from now on. Let furthermore $u(t, x, v)$ indicate the density of tips at time t, location x and velocity v. Then the marginal tip density at a certain location and a certain time reads

$$\overline{u}(t, x) = \int_V u(t, x, v)\, dv.$$

In accordance with data, we assume the tips to grow almost in straight lines (a tip that once has chosen a certain velocity v keeps this velocity for all times), and to split at a given rate λ. This is, the spontaneous change of direction of a tip happens at a very small rate ε, while the new direction is in a narrow cone around the old direction, given by the kernel $K_1(v, v')$. We assume that tips are able to measure the tip density: the velocity γ as well as the branching rate λ depend on $\overline{u}$, $\gamma = \gamma(\overline{u})$, $\lambda = \lambda(\overline{u})$; we will discuss this assumption later on. The functions $\gamma(.)$ and $\lambda(.)$ are non-increasing functions on $\overline{u}$. The new tip selects the velocity in dependence of the velocity of the "mother" tip. Given the velocity v' of the mother, the velocity distribution of the daughter tip is given by the kernel $K_2(v, v')$. We find that the split branches do not start to grow at once, but that there is almost always a considerable delay. The tips first grow at a lower rate until they gain velocity and eventually grow with the same rate like the primary tips. We model this effect simply as a delay $r \geq 0$ in the start of the growth. This is for sure only a simplifying assumption; a distribution of velocities, depending on the age of a tip, would be more appropriate. As we do not expect the conclusions to change essentially by the simplifications made here, we stick to this more simple model. A direct simulation of the stochastic process (with more or less arbitrary parameters) and a microscopic image of *Phytophthora* can be found in Fig. 1. For simplicity, we did choose especially $\varepsilon = r = 0$. We find a structural similarity in the the morphology of *Phytophthora* and the simulation.

All in all, we describe the spread of tips by the equation

$$
\begin{aligned}
u_t(t, x, v) + (v^T \nabla) & \left[\gamma(\overline{u}(t, x)) u(t, x, v) \right] \\
&= \varepsilon \left(-u(t, x, v) + \int_V K_1(v, v') u(t, x, v')\, dv' \right) \\
&\quad + \lambda(\overline{u}(x, t - r)) \int_V K_2(v, v') u(t - r, x, v')\, dv'
\end{aligned}
\tag{1}
$$

for all $v \in \mathbb{S}^1$.
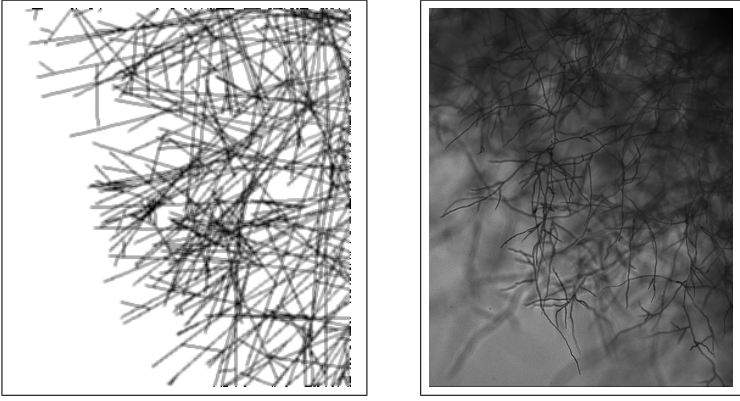
Fig. 1 Simulation of the stochastic process (left panel, $\varepsilon = 0$ and $r = 0$) and microscopic image of *Phytophthora* (right panel).

3 Running fronts

We aim at a basic understanding of the running fronts that our model may exhibit. In order to obtain analytic results and some insight into the fundamental structure, we first consider an extreme case yielding an equation simple enough to be analytically treatable. However, let us first define what we understand by a "front" in the present context.

Definition 1 A nonnegative function $U(\tau, v)$ is denoted as a *front* with velocity $c \in [0, \sup_{\zeta \in \mathbb{R}_+} \gamma(\zeta)]$, provided $u(t, x, v) = U(x_1 - ct, v)$ is non-trivial, solves (1), and satisfies the relations $U(\infty, v) \equiv 0$, $\int_{\mathbb{S}^1} U(\tau, v)\, dv < \infty$.

Given a front U for the differential equation (1) with constant functions γ, λ, we see that U fulfills

$$
(\gamma v_1 - c)\partial_\tau U(\tau, v) + \varepsilon U(\tau, v)
$$
$$
= \varepsilon \int_V K_1(v, v') U(\tau, v')\, dv' + \lambda \int_V K_2(v, v') U(\tau + cr, v')\, dv'
$$

with $v = (v_1, 0)$ and $\tau = x_1 - ct$.

3.1 Constant kernels

In this subsection, we replace the kernels in our model (1) by a uniform distribution, i.e. $K_i(v, v') \equiv 1/(2\pi)$ for $i = 1, 2$, and thus (1) reduces to

$$
u_t(t, x, v) + (v^T \nabla)\left[\gamma(\overline{u}(t, x)) u(t, x, v)\right]
$$
$$
= \varepsilon \left(-u(t, x, v) + \frac{1}{|V|}\overline{u}(x, t)\right) + \frac{\lambda(\overline{u}(x, t - r))\ \overline{u}(x, t - r)}{|V|}. \quad (2)
$$

If we discard the delay, we are in the classical case of the velocity-jump process. The assumption of $K_i(v, v') \equiv$ constant further simplifies the situations, s.t. we come close to the equations considered in the papers [35,36]. The difference is that we allow for an unbounded growth — the tips split, but are never annihilated. For the convenience of the reader, we repeat here the computations made in [35,36] that determine the velocity of the front.

Remark 1 As we allow for an unbounded growth, we cannot expect the solution to go to an stationary state for $\tau \to -\infty$. Also the classical linear diffusion equation $h_t = \Delta h + \alpha h$ possesses running fronts with minimal velocity $2\sqrt{\alpha D}$ that are unbounded for $x \to -\infty$.

Theorem 1 *Let the functions λ, γ be constant. If a differential equation (2) possesses a front of the form*

$$\overline{U}(\tau) := \int_V U(\tau, v)\, dv = Ce^{-\sigma\tau} \tag{3}$$

for some real $C, \sigma > 0$, $\sigma = \sigma(c)$, then one has $c \in \left[\gamma\sqrt{1 - \frac{\varepsilon^2}{(\lambda+\varepsilon)^2}}, \gamma\right)$ and $\sigma \in \{\sigma_r^-, \sigma_r^+\}$ with:

(a) If $r = 0$, then $\sigma_0^\pm = \frac{\varepsilon c \pm \sqrt{\varepsilon^2 c^2 - \lambda(\gamma^2 - c^2)(2\varepsilon + \lambda)}}{\gamma^2 - c^2}$,
(b) if $r > 0$, then $\sigma_r^- \in (0, \sigma_0^+)$ is decreasing in r, while $\sigma_r^+ \in (\sigma_0^+, \frac{\varepsilon}{\gamma-c})$ is increasing in r.

Proof Assume a front $U(\tau, v)$ with $\overline{U}(\tau) = Ce^{-\sigma\tau}$ exists. We may define the profile of the front

$$w(\tau, v) = U(\tau, v)/\overline{U}(\tau).$$

For $\tau \in \mathbb{R}$ one has $w(\tau, \cdot) \in L^1(V)$ and $\int_V w(\tau, v)\, dv = 1$. The function $U(\tau, v)$ satisfies the equation

$$(\gamma v_1 - c)\partial_\tau U(\tau, v) + \varepsilon U(\tau, v) = \frac{\varepsilon}{|V|}\overline{U}(\tau) + \frac{\lambda}{|V|}\overline{U}(\tau + \hat{r})$$

with $\hat{r} = rc$. Using $U(\tau, v) = \overline{U}(\tau)w(\tau, v)$ and $\overline{U}'(\tau) = -\sigma\overline{U}(\tau)$, we obtain from the product rule

$$(\gamma v_1 - c)[-\sigma\overline{U}(\tau)w(\tau, v) + \overline{U}(\tau)\partial_\tau w(\tau, v)] + \varepsilon\overline{U}(\tau)w(\tau, v)$$
$$= \frac{\varepsilon}{|V|}\overline{U}(\tau) + \frac{\lambda}{|V|}\overline{U}(\tau + \hat{r}).$$

Dividing by $\overline{U}(\tau)$ yields (note that $\overline{U}(\tau + \hat{r})/\overline{U}(\tau) = e^{-\hat{r}\sigma}$)

$$(\gamma v_1 - c)[-\sigma w(\tau, v) + \partial_\tau w(\tau, v)] + \varepsilon w(\tau, v) = \frac{\varepsilon + \lambda e^{-\sigma\hat{r}}}{|V|}$$

and we find a solution constant in time, $w_0 = w_0(v)$ with

$$w_0(v) = \frac{\varepsilon + \lambda e^{-\sigma \hat{r}}}{|V|[\varepsilon + \sigma c - \sigma \gamma v_1]}.$$

A general solution can be represented by $w(\tau, v) = w_0(v) + \tilde{w}(\tau, v)$. For $\tilde{w}(\tau, v)$ we obtain

$$(\gamma v_1 - c)[-\sigma \tilde{w}(\tau, v) + \partial_\tau \tilde{w}(\tau, v)] + \varepsilon \tilde{w}(\tau, v) = 0.$$

This is, for v_1 given s.t. $\gamma v_1 - c \neq 0$, the function $\tilde{w}(\tau, v)$ is either 0 or tends to infinity for $t \to \infty$ or $t \to -\infty$ (depending on the sign of $\sigma - \frac{\varepsilon}{\gamma v_1 - c}$). However, it is not possible for $\tilde{w}(\tau, v)$ to grow exponentially fast in τ for a set of non-zero measure in V, to be non-negative, and to obey the condition $\int_V w(\tau, v)\, dv \equiv 1$. Thus, $\tilde{w}(\tau, v) = 0$, and we explicitly obtain the velocity profile of a front with exponent $-\sigma$ given by $w_0(v)$.

However, for c given, the exponent cannot be arbitrary but is selected by the integrability condition

$$1 = \int_V w_0(v)\, dv = \frac{\varepsilon + \lambda e^{-\sigma \hat{r}}}{|V|} \int_0^{2\pi} \frac{d\varphi}{\varepsilon + \sigma c - \sigma \gamma \cos(\varphi)} = \frac{\varepsilon + \lambda e^{-\sigma cr}}{\sqrt{(\varepsilon + \sigma c)^2 - (\sigma \gamma)^2}},$$

whose right hand side is denoted by $H_r(\sigma, c)$. First, this requires $\varepsilon + \sigma c > \sigma \gamma$, since for $\varepsilon + \sigma c \leq \sigma \gamma$, the integral diverges. We find $H_r(0, c) = 1 + \frac{\lambda}{\varepsilon} > 1$. Furthermore, $\lim_{\sigma \to \frac{\varepsilon}{\gamma - c}^-} H_r(\sigma, c) = \infty$. Thus, in order to obtain a solution of $H_r(\sigma, c) = 1$ in $\mathbb{R}^+$, it is necessary that there is $\sigma^* > 0$ s.t. $H_r(\sigma^*, c) \leq 1$.

Case 1: $r = 0$. In this case, $H_0(s, c) = 1$ is equivalent to the quadratic equation

$$(\gamma^2 - c^2)s^2 - 2\varepsilon cs + \lambda^2 + 2\varepsilon \lambda = 0 \tag{4}$$

having the discriminant $\delta := 4\varepsilon^2 c^2 - 4(\gamma^2 - c^2)(\lambda + 2\varepsilon)\lambda$. Thus, in order to guarantee a real solution to (4) we have to require $\delta \geq 0$, which implies $c \geq \gamma \sqrt{1 - (\frac{\varepsilon}{\varepsilon + \lambda})^2}$. Moreover, the explicit solutions to $H_0(\sigma, c) = 1$ read as

$$\sigma_0^{\pm} = \frac{\varepsilon c \pm \sqrt{\delta/4}}{\gamma^2 - c^2}.$$

Case 2: $r > 0$. Here it is not possible to determine the solutions of $H_r(\sigma, c) = 1$ in terms of elementary functions. However, we may write

$$H_r(\sigma, c) = \frac{\varepsilon + \lambda}{\sqrt{(\varepsilon + \sigma c)^2 - (\sigma \gamma)^2}} - \frac{\lambda(1 - e^{-\sigma cr})}{\sqrt{(\varepsilon + \sigma c)^2 - (\sigma \gamma)^2}} = H_0(\sigma, c) - h(\sigma).$$

Thus, $H_r(\sigma, c) < H_0(\sigma, c)$, and for continuity reasons there must be two solutions $\sigma_r^- \in (0, \sigma_0^-)$ and $\sigma_r^+ \in (\sigma_0^+, \frac{\varepsilon}{\gamma - c})$ to the equation $H_r(\sigma, c) = 1$ with the claimed properties. $\square$

Corollary 1 *If σ_r^* denotes the slope corresponding to the minimal velocity c_r^* determined by the conditions*

$$H_r(\sigma_r^*, c_r^*) = 1, \qquad D_1 H_r(\sigma_r^*, c_r^*) = 0, \tag{5}$$

then the following holds:

(a) If $r = 0$, then we obtain the relations

$$c_0^* = \gamma \sqrt{1 - \frac{\varepsilon^2}{(\lambda + \varepsilon)^2}} = \gamma \left(1 - \frac{\varepsilon^2}{2\lambda^2} + \mathcal{O}(\varepsilon^3) \right),$$

$$\sigma_0^* = \frac{(\lambda + \varepsilon)\sqrt{\lambda(\lambda + 2\varepsilon)}}{\gamma \varepsilon} = \frac{\lambda^2}{\gamma \varepsilon} + \mathcal{O}(\varepsilon).$$
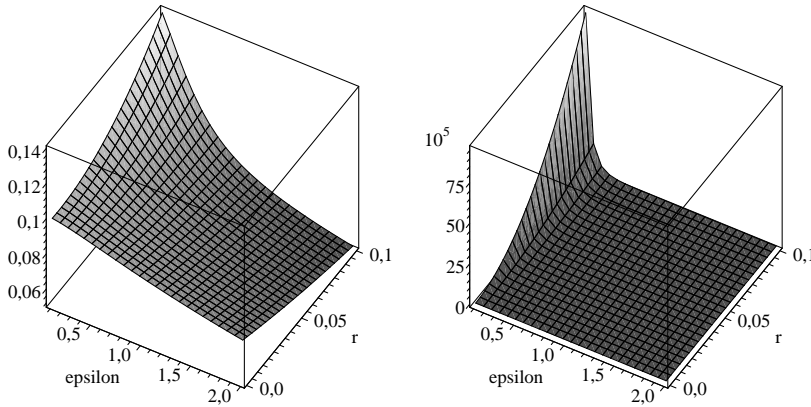
(b) If $r > 0$, then one has the expansions

$$c_r^* = c_0^* - \frac{\varepsilon \gamma \lambda^{3/2} \sqrt{\lambda + 2\varepsilon}}{(\varepsilon + \lambda)^2} r + \mathcal{O}(r^2), \qquad \sigma_r^* = \sigma_0^* - \frac{\lambda^{5/2}\sqrt{\lambda + 2\varepsilon}^3}{\gamma \varepsilon^2} r + \mathcal{O}(r^2).$$

showing that small delays $r > 0$ have a decreasing effect on the slope σ_r^* and the velocity c_r^*. Moreover, the asymptotic representation

$$\sigma_r^* \approx \frac{1}{r\gamma} \ln \sqrt{\frac{\lambda^2 r}{\varepsilon}}$$

holds true.

In Figure 2 we have depicted graphs for the Taylor expansions to c_r^* and σ_r^* as graphs of ε and r.

Fig. 2 Taylor approximation of c_r^* (left) and σ_r^* (right) in r up to order 2. For simplicity we have chosen the parameter values $\gamma = 0.1$ and $\lambda = 1$

Proof (a) For the sake of a brief notation we abbreviate $\mu := \frac{\varepsilon}{\lambda + \varepsilon}$ and use the notation from the proof of Theorem 1 throughout. The velocity c of a front with $r = 0$ is contained in the interval $[\gamma\sqrt{1 - \mu^2}, \gamma)$. It is thus only necessary to consider the lowest velocity $c^* = \gamma\sqrt{1 - \mu^2}$. We find that c_0^* is characterized by the fact that $H_0(\sigma, c)$ just touches the value one. This holds for a discriminant $\delta = 0$ and so

$$\sigma_0^* = \frac{\varepsilon c}{\gamma^2 - c^2}.$$

As $c = \gamma + \mathcal{O}(\varepsilon)$ and $\gamma^2 - c^2 = \gamma^2\varepsilon^2/(\varepsilon + \lambda)^2 = (\gamma\varepsilon/\lambda)^2 + \mathcal{O}(\varepsilon^3)$, we obtain

$$\sigma \sim \varepsilon^{-1}\frac{\lambda^2}{\gamma}.$$

We may also compute σ_0^* precisely from $H_0(\sigma, c^*) = 1$,

$$(\varepsilon + \lambda)^2 = (\varepsilon + \sigma c^*)^2 - (\sigma\gamma)^2 = (\varepsilon + \sigma\gamma\sqrt{1 - \mu^2})^2 - (\sigma\gamma)^2$$
$$= \varepsilon^2 + 2\varepsilon\sigma\gamma\sqrt{1 - \mu^2} - \sigma^2\gamma^2\mu^2$$

and this is

$$\sigma_0^* = \frac{2\varepsilon\gamma\sqrt{1 - \mu^2} \mp \sqrt{4\varepsilon^2\gamma^2(1 - \mu^2) + 4(\varepsilon^2 - (\varepsilon + \lambda)^2)\gamma^2\mu^2}}{2\gamma^2\mu^2}$$

$$= \frac{(\lambda + \varepsilon)\sqrt{\lambda(\lambda + 2\varepsilon)}}{\gamma\varepsilon}$$

(b) Inserting the relations $\sigma_r^* = \sigma_0^* + \sigma_1 r + \mathcal{O}(r^2)$, $c_r^* = c_0^* + c_1 r + \mathcal{O}(r^2)$ into our identities (5) for $r \geq 0$, yields two linear algebraic equations to determine the coefficients σ_1, c_1. We leave their solution to the interested reader, yielding the claimed expansions for σ_r^*, c_r^*.

We have

$$H_{\hat{r}}(\sigma, c) = \frac{\varepsilon + \lambda e^{-\sigma\hat{r}}}{\sqrt{(\varepsilon + \sigma c)^2 - (\sigma\gamma)^2}}$$

with the derivative

$$D_1 H_{\hat{r}}(\sigma, c) = \frac{-\hat{r}\lambda e^{-\sigma\hat{r}}}{\sqrt{(\varepsilon + \sigma c)^2 - (\sigma\gamma)^2}} - \frac{(\varepsilon + \lambda e^{\sigma\hat{r}})((\varepsilon + \sigma c)c - \sigma\gamma^2)}{[(\varepsilon + \sigma c)^2 - (\sigma\gamma)^2]^{3/2}}$$

$$= \frac{-\hat{r}\lambda e^{-\sigma\hat{r}}}{\varepsilon + \lambda e^{\sigma\hat{r}}}\frac{\varepsilon + \lambda e^{-\sigma\hat{r}}}{\sqrt{(\varepsilon + \sigma c)^2 - (\sigma\gamma)^2}}$$

$$\quad - \frac{(\varepsilon + \lambda e^{-\sigma\hat{r}})((\varepsilon + \sigma c)c - \sigma\gamma^2)}{(\varepsilon + \lambda e^{\sigma\hat{r}})^3}\frac{(\varepsilon + \lambda e^{-\sigma\hat{r}})^3}{[(\varepsilon + \sigma c)^2 - (\sigma\gamma)^2]^{3/2}}$$

$$= \frac{-\hat{r}\lambda e^{-\sigma\hat{r}}}{\varepsilon + \lambda e^{-\sigma\hat{r}}}H_{\hat{r}}(\sigma) - \frac{(\varepsilon + \sigma c)c - \sigma\gamma^2}{(\varepsilon + \lambda e^{-\sigma\hat{r}})^2}H_{\hat{r}}(\sigma, c)^3.$$

We aim at pairs (σ, c) satisfying (5). As $H_r(\sigma, c) = 1$, we therefore find

$$-(\varepsilon + \lambda e^{-\sigma\hat{r}})\hat{r}\lambda e^{-\sigma\hat{r}} = (\varepsilon + \sigma c)c - \sigma\gamma^2$$

and equivalently

$$0 = \sigma c^2 + \varepsilon c - [\sigma\gamma^2 - (\varepsilon + \lambda e^{-\sigma\hat{r}})\hat{r}\lambda e^{-\sigma\hat{r}}],$$

which we solve for c, and find

$$c = \frac{1}{2\sigma}\left[-\varepsilon \pm \sqrt{\varepsilon^2 - 4\sigma\left(-\sigma\gamma^2 + (\varepsilon + \lambda e^{-\sigma\hat{r}})\hat{r}\lambda e^{-\sigma\hat{r}}\right)}\right]$$

$$= \frac{1}{2\sigma}\left[-\varepsilon \pm \sqrt{\varepsilon^2 - 4\sigma(\varepsilon + \lambda e^{-\sigma\hat{r}})\hat{r}\lambda e^{-\sigma\hat{r}} + 4\sigma^2\gamma^2}\right].$$

Since $\hat{r}$ depends on c, this in fact is a fixed point relation for c. As we require $c \geq 0$, we choose the positive sign in front of the root. We use this result to formally eliminate c from the equation $H_{\hat{r}}(\sigma, c) = 1$, and find

$$1 = H_{\hat{r}}(\sigma, c) = \frac{\varepsilon + \lambda e^{-\sigma\hat{r}}}{\sqrt{(\varepsilon + \sigma c)^2 - (\sigma\gamma)^2}}$$

$$= \frac{\varepsilon + \lambda e^{-\sigma\hat{r}}}{\sqrt{(\varepsilon - \frac{\varepsilon}{2} + \frac{1}{2}\sqrt{\varepsilon^2 - 4\sigma(\varepsilon + \lambda e^{-\sigma\hat{r}})\hat{r}\lambda e^{-\sigma\hat{r}} + 4\sigma^2\gamma^2})^2 - (\sigma\gamma)^2}}$$

$$= \frac{\varepsilon + \lambda e^{-\sigma\hat{r}}}{\sqrt{(\frac{\varepsilon}{2} + \frac{1}{2}\sqrt{\varepsilon^2 - 4\sigma(\varepsilon + \lambda e^{-\sigma\hat{r}})\hat{r}\lambda e^{-\sigma\hat{r}} + 4\sigma^2\gamma^2})^2 - (\sigma\gamma)^2}},$$

which is equivalent to

$$\left[\varepsilon + \lambda e^{-\sigma\hat{r}}\right]^2 = \left(\frac{\varepsilon}{2} + \frac{1}{2}\sqrt{\varepsilon^2 - 4\sigma(\varepsilon + \lambda e^{-\sigma\hat{r}})\hat{r}\lambda e^{-\sigma\hat{r}} + 4\sigma^2\gamma^2}\right)^2 - (\sigma\gamma)^2. \quad (6)$$

Any non-negative root of this equation together with the definition of σ in dependence on c leads to a solution (σ, c) that solves (5).

For $\varepsilon \searrow 0$, this equation becomes

$$\left[\lambda e^{-\sigma\hat{r}}\right]^2 = -\sigma\hat{r}\left(\lambda e^{-\sigma\hat{r}}\right)^2 + \sigma^2\gamma^2 - (\sigma\gamma)^2 = -\sigma\hat{r}\left(\lambda e^{-\sigma\hat{r}}\right)^2,$$

which implies for any $\sigma(\varepsilon)$ that possesses a finite limit,

$$\lim_{\varepsilon \searrow 0} \sigma(\varepsilon) = -1/\hat{r}.$$

With this result, we are able to compute c in the limit $\varepsilon \searrow 0$, and find

$$\lim_{\varepsilon \searrow 0} c(\varepsilon) = \frac{\hat{r}}{2}\sqrt{4\lambda^2 e^2 + 4\gamma^2/\hat{r}^2} = \sqrt{\gamma^2 + \lambda^2\hat{r}^2 e^2}.$$

This is, all solutions for σ that stay finite become negative and correspond to fronts with a velocity larger than γ. These solutions are not biologically feasible. As we know that there is a non-negative solution for all $\varepsilon > 0$, this solution cannot stay finite (otherwise one would find a sequence $\varepsilon \searrow 0$ with a

converging sequence $\sigma(\varepsilon_n)$, which eventually becomes non-feasible according to the argument above). This is,

$$\lim_{\varepsilon \searrow 0} \sigma(\varepsilon) = \infty. \tag{7}$$

For the sake of a more precise understanding of this limit relation, let us consider (6), which explicitly becomes

$$\varepsilon^2 + 2\varepsilon\lambda e^{-\sigma\hat{r}} + (\lambda e^{-\sigma\hat{r}})^2 = \gamma\varepsilon\sigma + \frac{\varepsilon^2}{4} - \sigma\left(\varepsilon + \lambda e^{-\sigma\hat{r}}\right)\hat{r}\lambda e^{-\sigma\hat{r}}$$
$$+ \left(\frac{\varepsilon}{2} + \frac{\varepsilon}{8\sigma\gamma}\right)^2$$
$$- \left(\frac{\varepsilon}{2} + \frac{\varepsilon}{8\sigma\gamma}\right)\frac{\left(\varepsilon + \lambda e^{-\sigma\hat{r}}\right)\hat{r}\lambda e^{-\sigma\hat{r}}}{\gamma}.$$

Being interested in the behavior for $\varepsilon > 0$ close to 0, due to (7) we obtain that $e^{-\sigma\hat{r}}$ is small. Hence, restricting to the dominant terms in the above equation yields

$$0 \approx \gamma\varepsilon\sigma - \sigma\left(\varepsilon + \lambda e^{-\sigma\hat{r}}\right)\hat{r}\lambda e^{-\sigma\hat{r}},$$

which is equivalent to $\sigma \approx \frac{1}{2\hat{r}}\ln\left(\frac{\lambda^2\hat{r}}{\gamma\varepsilon}\right)$. Keeping in mind that $c_r^* = c = \gamma + \mathcal{O}(\varepsilon)$ as $\varepsilon \searrow 0$ we obtain the claimed asymptotic representation of $\sigma = \sigma_r^*$. $\quad\square$

Remark 2 (a) We do not intend to prove the existence of the fronts described by the theorem above, nor the non-existence of other fronts. This task can be attacked by methods that mimic the work in [35, 36].

(b) If $r = 0$ and there exists a running front (3) with velocity $\gamma = c$, then

$$\sigma = \frac{\lambda}{\gamma}\left(1 + \frac{\lambda}{2}\varepsilon^{-1}\right).$$

If we consider the limit $\varepsilon \to 0$, the slope of the interface develops a singularity, and the front fails to exist in the limit.

(c) A similar result can be obtained, if we ask for all fronts $U(v, \tau)$ that can be written in a product form,

$$U(v, \tau) = \overline{U}(\tau)\,w_0(v).$$

Provided both factors are differentiable, then we obtain exactly the fronts described in Theorem 1.

(d) We expect that no front with a smaller velocity than the minimal velocity exists. We furthermore expect that the front with minimal velocity is stable. This conjecture is based on similar results found for running fronts obtained in [35].

3.2 General Kernels

We now drop the assumption that the kernels K_i, $i = 1, 2$, in (1) are constant and assume that they are essentially bounded. Our arguments are based on the Krein-Rutman theorem which requires function spaces with solid cones, like for instance continuous functions,

$$C_+(V) := \{w \in C(V) : w(v) \geq 0 \text{ for all } v \in V\}.$$

Let us assume that the integral operators

$$\mathbf{K}_i : C(V) \to C(V), \quad w \mapsto \int_V K_i(v, v') w(v')\, dv', \qquad i \in \{1, 2\}$$

are compact, which holds for kernels K_i satisfying the continuity assumption

$$\lim_{v \to v_0} \int_V |K_i(v, v') - K_i(v_0, v')|\, dv' = 0 \quad \text{for all } v_0 \in V \tag{8}$$

(cf. [25, p. 247, Thm. 3']). An example is a kernel of finite rank,

$$K_i(v, v') = \sum_{j=1}^n g_j^i(v) h_j^i(v'),$$

where the nonnegative functions g_j^i are continuous, h_j^i are chosen to be in $L^1(V)$, and obey the condition

$$1 = \int_V K_i(v, v')\, dv' = \sum_{j=1}^n g_j^i(v) \int_V h_j^i(v')\, dv'.$$

Let us assume that both kernels K_i are strictly positive.

Theorem 2 *Let the functions λ, γ be constant and suppose the kernels K_i satisfy (8). If (1) possesses a front of the form (3), then there is a $\kappa^*(\varepsilon, r)$ s.t. for each velocity $c \in [\kappa^*, \gamma)$ a running front with the above shape (3) exists.*

Proof Let us assume a front $U(\tau, v)$ with $\overline{U}(\tau) = Ce^{-\sigma\tau}$ exists. As in Theorem 1 we may define the profile of the front

$$w(\tau, v) = U(\tau, v)/\overline{U}(\tau)$$

for $\tau \in \mathbb{R}$, $w(\tau, \cdot) \in C(V)$ and $\int_V w(\tau, v)\, dv = 1$. The function $U(\tau, v)$ satisfies the equation

$$(\gamma v_1 - c)\partial_\tau U(\tau, v) + \varepsilon U(\tau, v)$$
$$= \varepsilon \int_V K_1(v, v') w(\tau, v')\, dv' \overline{U}(\tau) + \lambda \int_V K_2(v, v') w(\tau + \hat{r}, v')\, dv' \overline{U}(\tau + \hat{r})$$

with $\hat{r} = cr$. We apply the relations $U(\tau, v) = \overline{U}(\tau)w(\tau, v)$, $\overline{U}'(\tau) = -\sigma\overline{U}(\tau)$, from which the product rule implies

$$(\gamma v_1 - c)[-\sigma\overline{U}(\tau)w(\tau, v) + \overline{U}(\tau)\partial_\tau w(\tau, v)] + \varepsilon\overline{U}(\tau)w(\tau, v)$$
$$= \varepsilon\overline{U}(\tau)\int_V K_1(v, v')w(\tau, v')\,dv' + \lambda\overline{U}(\tau + \hat{r})\int_V K_2(v, v')w(\tau + \hat{r}, v')\,dv'$$

We again divide by $\overline{U}(\tau)$ and deduce (we observe $\overline{U}(\tau + \hat{r})/\overline{U}(\tau) = e^{-\hat{r}\sigma}$)

$$(\gamma v_1 - c)[-\sigma w(\tau, v) + \partial_\tau w(\tau, v)] + \varepsilon w(\tau, v)$$
$$= \varepsilon\int_V K_1(v, v')w(\tau, v')\,dv' + \lambda e^{-\sigma\hat{r}}\int_V K_2(v, v')w(\tau + \hat{r}, v')\,dv'.$$

We find a solution constant in time, $w_0 = w_0(v)$ with

$$w_0(v) = \int_V \frac{\varepsilon K_1(v, v') + \lambda e^{-\sigma\hat{r}}K_2(v, v')}{[\varepsilon + \sigma c - \sigma\gamma v_1]}\,w_0(v')\,dv' =: T_\sigma[w_0](v).$$

Due to our assumption (8) the operator $T_\sigma : C_+(V) \to C_+(V)$ is strongly positive and compact. We thus may use the Theorem of Krein-Rutman (see, e.g., [44, p. 290, Thm. 7.C]) and find that a velocity profile exist if and only if the spectral radius fulfills $\rho(T_\sigma) = 1$. Let us consider the spectral radius closer.

If $\sigma = 0$, we find

$$T_0[w] = \int_V K_1(\cdot, v')w(v')\,dv' + \frac{\lambda e^{-\sigma\hat{r}}}{\varepsilon}\int_V K_2(\cdot, v')w(v')\,dv'.$$

Integrating over v yields $\int_V T_0[w](v)\,dv = (1 + \frac{\lambda e^{-\sigma\hat{r}}}{\varepsilon})\int_V w_0(v')\,dv'$, this is, $1 \in L^\infty$ is a left-eigenfunction (or eigenfunction for the adjoint operator) for eigenvalue $\rho(T_0) = 1 + \frac{\lambda e^{-\sigma\hat{r}}}{\varepsilon} > 1$. In the limit $\sigma \to \frac{\varepsilon}{\gamma - c}-$, we have $\rho(T_\sigma) \to \infty$, as the kernel develops a pole of first order. All in all, for a valid velocity profile to exist we need to show that there is $\sigma^* \in (0, \frac{\varepsilon}{\gamma - c})$ s.t. $\rho(T_{\sigma^*}) < 1$.

If we define $u_0(v) = [\varepsilon + \sigma c - \sigma\gamma v_1]w_0(v)$, we find

$$u_0(v) = \int_V \frac{\varepsilon K_1(v, v') + \lambda e^{-\sigma\hat{r}}K_2(v, v')}{[\varepsilon + \sigma c - \sigma\gamma v_1']}\,u_0(v')\,dv' =: \hat{T}_{\sigma,c}[u_0](v).$$

We again focus on Perron eigenvalues for the operator $\hat{T}_{\sigma,c} : C_+(V) \to C_+(V)$. Let us assume that for $c_1 \in (0, \gamma)$ an eigenfunction for eigenvalue 1 in $C_+(V)$ exist, if we select $\sigma = \sigma_1 > 0$ in an appropriate way. Consider $c \in (c_1, \gamma)$. For monotonicity reasons,

$$\rho(T_{\sigma_1, c}) \leq \rho(T_{\sigma_1, c_1}) = 1.$$

Note that a Perron eigenvalue $\rho(T_{\sigma, c})$ of the compact operator $\hat{T}_{\sigma, c}$ depends continuously on σ for $c \in (0, \gamma)$ fixed. As $\rho(T_0) > 1$ we find some σ_2 s.t. $\rho(T_{\sigma_2, c}) = 1$. This is, the set of allowed velocities forms an interval $[\kappa^*(\varepsilon, r), \gamma)$ or $(\kappa^*(\varepsilon, r), \gamma)$. Due to continuity reasons, the smallest velocity is included into the set of allowed velocities. This is the first part of the proof.

Next we want to prove that there is an interval of admissible velocities, indeed. Therefore, take $r = 0$, and use the boundedness of the contact kernels, $K_i(v, v') \leq k$ to obtain the upper bound

$$T_{\sigma,c}[u] \leq \left(\varepsilon k + \lambda e^{-\sigma \hat{r}} k\right) \int_V \frac{u(v')}{[\varepsilon + \sigma c - \sigma \gamma v_1']} \; dv' =: G_1[u](v').$$

The comparison principle of positive, compact operators (see, for instance, [44, p. 291, Cor. 7.28]) yields $\rho(T_{\sigma.c}) \leq \rho(G_1)$. As $G_1[.]$ is a rank-one operator (all functions are mapped to a constant function), the spectral radius reads

$$\rho(G_1) = G_1[1] = \int_V \frac{1}{[\varepsilon + \sigma c - \sigma \gamma v_1']} \; dv' = \frac{\varepsilon k + \lambda e^{-\sigma \hat{r}} k}{\sqrt{(\varepsilon + \sigma c)^2 - (\sigma \gamma)^2}} =: \tilde{H}_r(\sigma; c)$$

The analysis above (see the proof of Theorem 1) reveals that the minimum of $\tilde{H}_0(\cdot; c)$ is assumed at $\sigma^* = \frac{\varepsilon c}{\gamma^2 - c^2}$, and

$$\tilde{H}_r(\sigma^*; c) = \left(\varepsilon k + \lambda e^{-\sigma \hat{r}} k\right) \sqrt{1 - (c/\gamma)^2} \leq H_0(\sigma^*; c)$$

This is, if we let c be arbitrary close to γ, then $\rho(T_{\sigma,c}) \leq 1$, and thus c is a feasible strategy for all $r > 0$. $\quad\square$
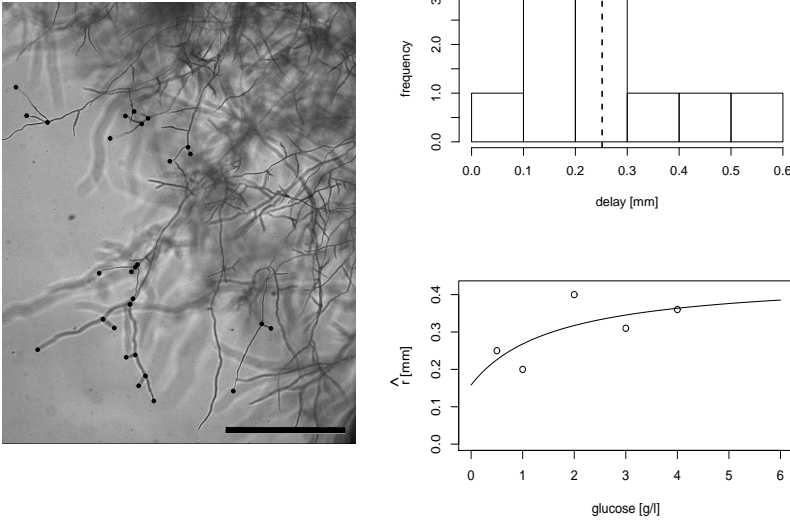
Fig. 3 Measurement of the delayed growth. Left hand side: the end points and branching points of some hyphae (indicated by solid dots) are used to estimate the length difference of mother/daughter branches. The bar is one mm. Right hand side, upper panel: histogram of the absolute value of the length difference between mother-daughter hyphae (0.5 g/L glucose). The dotted vertical bar indicates the mean value. Right hand side, lower panel: Dependency of the mean value for the delay on the glucose concentration.

4 Material and methods

Next we aim to confirm our theoretical predictions using tangible experiments in Petri dishes. For this, *Phytophthora plurivora* was grown in Petri dishes on M1-agar and in M1-liquid media for examination under microscope using varied concentrations of glucose. M1 was a chemically defined medium which contained (g/L): L-asparagine, 0,2; CaCl2, 0.01; FeSO4*7H2O, 0.001; MgSO4*7H2O, 0.0001; KH2PO4, 0.47; K2HPO4, 0,26; thiaminhydrocloride, 0.001; ZnSO4*7H2O, 0.001; CuSO4*5H2O, 0.00002; NaMoO4*2H2O, 0.00002; MnCl4*4H2O, 0.00002 and D-glucose varying from 0 up to 21 g/L adding 10 g/L agar to get solid media for usage in Petri dishes. The general conditions like humidity, and temperature which was set on 20^0C have been kept constant. The daily increment of hyphal growth of each glucose-treatment was 2D-recorded in a centre line cross on the bottom side of every Petri dish. For optical analysis 5 Petri dishes were scanned with transmitting light, digitized and analyzed via Image-J (graphical software, [1]). Additionally eight abutted pieces along these cross lines were punched out from agar with a cork borer to verify the consumption of glucose during hyphal expansion. Every four with the same distance to the centre of the culture from the same dish became one pooled sample, which was immediately frozen in -80^0C, lyophilized and grinded in a ball mill. After adding 1mL of double-distilled water, the liquid with the solved glucose was filtered through syringe filters and analyzed by high performance liquide chromatography (HPLC) consisting of an autosampler (S5200, Schambeck SFD, Bad Honnef, Germany), a HPLC-pump (SDS 9404, Schambeck SFD), a column oven (SFD 12560, Schambeck SFD), as well as a refractive index detector (RI-2000, Schambeck-SFD). Separation of 20 μL of samples was performed on a CARBOsep CHO-820 calcium column (Transgenomic, Glasgow, UK) maintained at 85^0C. Outgased Millipore water was used as a solvent at a constant flow rate of 0.6 mL min-1. Data acquisition and calculation were performed with the System Gold Nouveau software (Beckman, Krefeld, Germany). Calibration of the retention times needed for identification and quantification was done with dilution series of standard solutions in five different concentrations (0.2, 0.4, 0.6, 1,0 or 2,5 $mgmL^{-1}$) containing glucose. The resulting glucose concentration was related to the original volume of the used pieces of agar. To test whether hyphae are producing a toxic or growth inhibiting substance, the paper filtered liquid of M1-media in which *Phytophthora* was grown has been added to new Petri dishes with M1-agar before inoculation. Finally, the growth was compared with a control where dishes were just treated with water.

5 Parameter estimation

We obtain three parameters (delay, growth rate, split rate) and the exponent of the interface of the front. This information is interesting as the theory yields a prediction of the exponent of a front, given the growth, the split rate, the

delay and the rate at which a tip changes direction. The last parameter is very small, so that we may use this theoretical relation as a validation for the model developed.

Delay. In order to obtain an information about the magnitude of the delay, we compared the length of a split depending on the growing behavior in different concentrations of glucose in M1-media. The length difference between the two branches is correlated with the delay (see Fig. 3). There are several problems in this simple method: we approximate the hyphae by straight lines between branching- and end-points, we can only recognize vaguely if a hyphae bows away from the focus plane, and the hyphae measured are selected arbitrarily and not systematically, bearing the danger of a subjective bias. These effects may lead to a wrong estimation of length and thus a wrong estimation of the delay. It is necessary to keep all these problems in mind, in interpreting the resulting function

$$\hat{r}(g) = 0.16 \text{ mm} + \frac{0.29 \ g \ \text{mm}}{g + 1.64 \text{ g/L}}.$$

Please note that g (italic) denotes the glucose concentration, while g refers to the unit "gram". This is, $[g] = $ g/L.

It is clear that a random delay, stochastically distributed, would be more appropriate than the fixed delay chosen in the present model. However, the approach chosen yields some acceptable estimation.

Velocity. The overall velocity of spread has been measured using the spread of *Phytophthora* in M1-agar with various glucose concentrations. Although in a radial symmetric setting, *Phytophthora* spreads in a uniform manner. As we know from microscopic images that the hyphae grow rather in straight lines, we expect the overall growth velocity to be close to the growth velocity of single hyphae. Please note that there is still growth at zero glucose concentration, as the *Phytophthora* are able to utilize a second carbon source (asparagine). We obtain a functional dependence of the velocity on the glucose concentration in the agar (Fig. 4),

$$\gamma(g) = \left(2.7 + 1.5 \, e^{-0.723 \, g/(\text{g/L})}\right) \ \ \text{mm/day};$$

this function is chosen for phenomenological reasons only.

Split rate. The time course of the number of tips — given a certain glucose concentration — has been determined, and fit by an exponential function. The rates have been fitted in dependence on the available glucose rate, using a Hill function. We obtain (Fig. 5),

$$\lambda(g) = \frac{11.35 \ g^{4.6}/ \ \text{day}}{g^{4.6} + (0.96 \ \text{g/L})^{4.6}}.$$

Change of direction. It is hard to come up with a precise value for the rate at which the the hyphae change the direction of growth. Approximately,
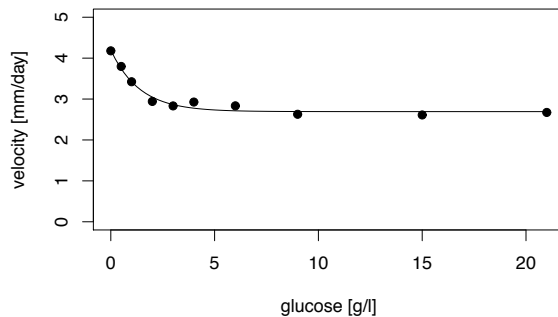
Fig. 4 Velocity of hyphae in dependence of glucose concentration.

they grow in straight lines. Thus, we chose (in comparison with λ, which is for glucose concentrations above 2g/L roughly 10/day) a rather small rate, $\varepsilon = 1$/day. This is, the change of direction is assumed to happen 10 times slower than the branching.
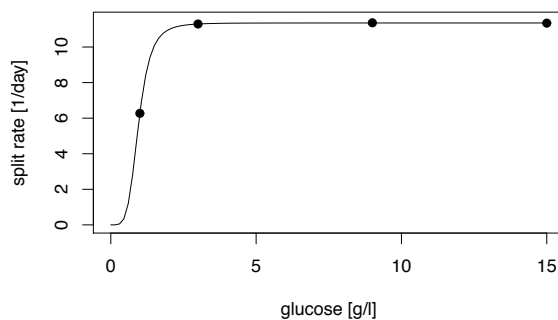

Fig. 5 Split rate of tips in dependence of glucose concentration.

Validation. The theory predicts the slope of the interface in dependence of λ, γ and ε via Corollary 1. In order to check this prediction, we determine the slope of the interface (see Fig. 6). Then, we plot the slope of the interface over the glucose concentration, together with the prediction of the theory (Fig. 7). The use of the "best fit" for delay $\hat{r}(g)$ yields an overestimation of the slope. If we use a delay two times higher, $2\hat{r}(g)$, and at the same time a halved split rate, $\lambda(g)/2$, we obtain the solid curve that fits surprisingly well. The factor 2 can be explained by the fact that the model used to obtain the
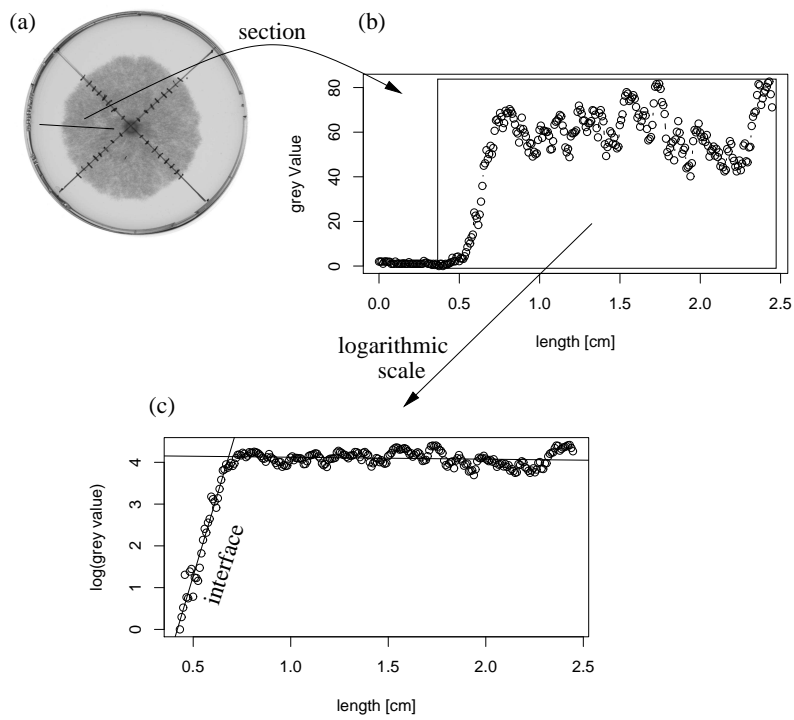
Fig. 6 Procedure to determine the exponent of the interface of the front. (a) A section of the grey values is taken. (b) A window containing the interface is selected, and (c) on a logarithmic scale the data can be approximated using two linear functions.
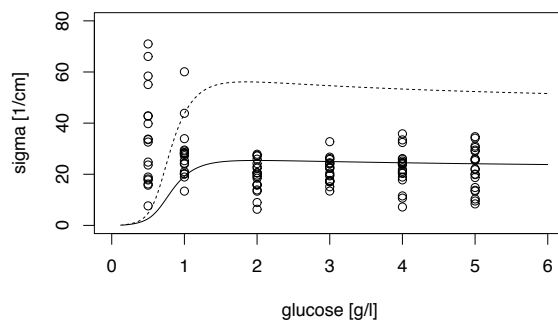
Fig. 7 Exponent of the interface of the front. Points: measurements, dashed curve: model prediction for the delay fitted, solid curve: model prediction for a delay two times higher, and split rate halved in comparison with the fitted functions.

slope assumes that all kernels are uniformly distributed on $\mathbb{S}^1$. However, if we consider the "true" kernel for branching, we find its mass concentrated on angles in $[-\pi/2, \pi/2]$. Only after several (two) branches, the direction of the tip has no correlation with the direction of its ancestor tip. If we only consider every nth split, we need to multiply the delay by n, and the split rate by $1/n$.

Most likely, the parameter of the model (especially the split rate for tips) is not appropriate any more if the glucose concentration is below one gram per liter. Especially the split rate enters in a crucial way the equation; and the split rate is hard to determine for small glucose concentrations as the the filament of *Phytophthora* becomes scanty.

6 Spatial simulations

Now we extend the model (1) from above by the influence of glucose. In order to obtain a simple simulation model, we suppress the dependencies of the rates on glucose, but consider the following model

$$u_t(t,x,v) + (v^T \nabla)\left[\gamma u(t,x,v)\right] = \varepsilon \left(-u(t,x,v) + \int_V K_1(v,v')u(t,x,v')\,dv' \right)$$

$$+ \hat{\lambda}(\overline{u}(x,t-r), \overline{u}(x,t)) \int_V K_2(v,v')u(t-r,x,v')\,dv' \qquad (9)$$

with

$$\hat{\lambda}(\overline{u}(x,t-r), \overline{u}(x,t)) = \lambda(u_{max} - \overline{u}(x,t))_+\overline{u}(x,t-r).$$

Here, u_{max} is an upper bound suggested by the data (see Fig. 6). This model is augmented by the diffusion equation for glucose,

$$g_t = D\Delta g - \mu\overline{u}(x,t)$$

with no-flux boundary conditions and initial condition $g(x,0) = g_0$. Below we will extent this model further, incorporating a feedback from glucose to tips. For the moment, we assume that glucose depletion does not play a role. Note that we only consider tips, not hyphae. Though we basically assume no explicit dependency of the parameters on the glucose concentration (we use approximately the values obtained in the last section for glucose levels above one gram per liter glucose) and only use fitting by eye, we obtain a reasonable agreement between experiment and model (see Fig. 8). The parameter values can be found in Tab. 1.

At this point, we want to make three comments:

(a) The numerical scheme used led to a certain spatial anisotropy caused by the grid the scheme is based on.
(b) The diffusion coefficient is in agreement with Matsunaga et al. [26] when taking into account that they measured at 37^0C but using twice as much of agar in their membrane. We assume that this is a fixed coefficient when using for D.
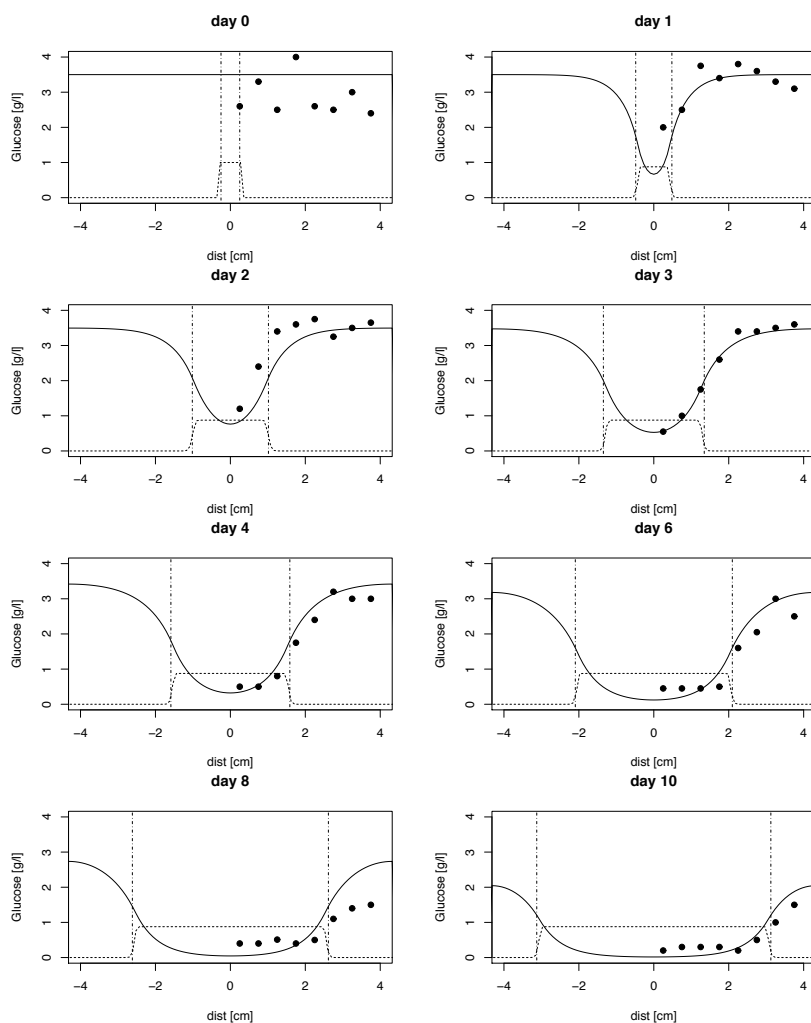
Fig. 8 Spatial model. The solid points are measurements of glucose concentration, the solid line the concentration predicted by the model. The dash-dotted vertical lines denote the edge of the front taken from the experiment, the dotted line the concentration of tips according to the model.

(c) In the early phase, i.e. up to day 1.55 (resp. between day 1 and day 1.55), glucose consumption resp. velocity is increased by a factor 4.5. This assumption is in line with experimental experience. Most likely, the agar plug used to inoculate the agar with *Phytophthora* provides enough nutrient to influence the spread in the initial phase. This observation may also be connected with a better diffusive transport in that stage of the experiments.

Variable	Value	Meaning
D	$0.55 \ 10^{-6}$ cm^2/sec	diffusion coefficient
g_0	3.5 g/l	initial glucose concentration
γ	0.278 cm/day	maximal velocity*
λ	11/day	split rate
ε	1.5/day	turning rate
u_{max}	1 U	maximal tip concentration in arbitrary units
μ	3/(U day)	glucose consumption rate per tip and day
$\hat{g}$	0.5 g/l	below this glucose level growth and splitting stops (only model 2)

Table 1 Values used in the spatial model (*Please note that in the initial phase a higher velocity had to be assumed, see text).

However, though the geometry of the simulations is slightly skewed, and the two conditions are not completely consistent, we expect the simulations to give at least semi-quantitative, valid results.
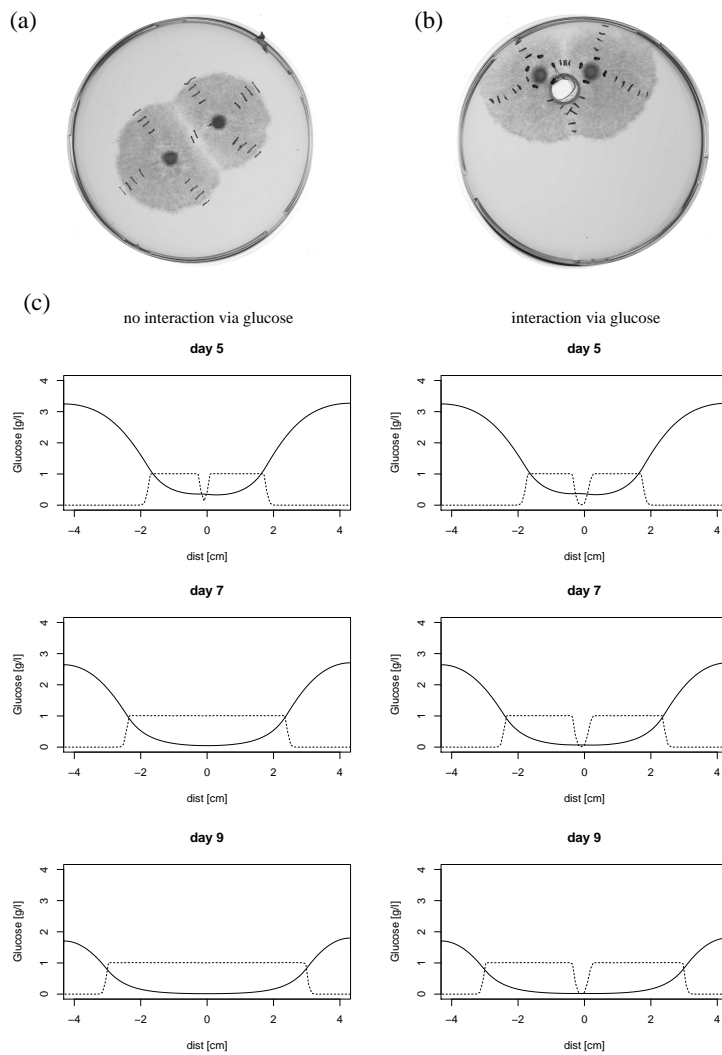
In order to obtain a deeper understanding of the interaction mechanisms between tips, confrontation experiments have been performed: two colonies have been placed in one Petri dish. After a few days, the colonies did grow close. Interestingly enough, the colony growth stops at the point where the colonies almost touch. There are several mechanisms possible that could lead to this behavior: (1) glucose drops below a critical level, (2) tips excrete a substance that inhibits growth and becomes high concentrated in-between the colonies, or (3) mechanical communication between tips, to name but a few.

The results of the experiments suggest that there is no significant inhibitory effect of exudates. And as the colonies do not meet in frontal manner but adjoin side by side after rounding an object Fig. 9b, the most basic assumption, and thus the first assumption that is to check, is that growth and movement of *Phytophthora* stops if the glucose concentration drops below a certain level.

Figures 4 and 5 indicate that velocity and split rate drops suddenly at glucose concentration somewhere between 0 and 1 gram per liter. We extend the model above by a feedback from glucose to tip dynamics. Due to simplicity, we use an extreme caricature of the observation, and take growth and split rate to 0 below a certain value in defining

$$\hat{\lambda}(\overline{u}(x,t-r),\overline{u}(x,t),g) = \lambda(u_{max} - \overline{u}(x,t))_+ \overline{u}(x,t-r) \, H(g-\hat{g}) \quad (10)$$
$$\gamma(g) = \gamma H(g-\hat{g})$$

where $H(x)$ denotes the Heaviside function, that is 0 for x negative and one elsewhere. This is, if the glucose is above a certain level $\hat{g}$, the behavior is like that of the basic model, while there is no splitting and no growth at glucose levels below $\hat{g}$. Apart of this feedback loop, the parameters are the same like before (see Tab. 1). The results are shown in Fig. 9c. The densities are displayed on a one-dimensional section through the colony centers. At the left hand side, we kept the model (9), while we show at the right hand side the version with influence of glucose depletion on splitting rate and growth, according to (10) with critical glucose level of $\hat{g} = 0.5$g/liter. We find a nice

(a)　　　　　　　　　　　　　　　　　　　　(b)

(c)

no interaction via glucose　　　　　　　　　interaction via glucose

day 5　　　　　　　　　　　　　　　　　　**day 5**

day 7　　　　　　　　　　　　　　　　　　**day 7**

day 9　　　　　　　　　　　　　　　　　　**day 9**

Fig. 9 Confrontation experiments. (a) Petri dishes with two colonies after 6 days with initial colony distance about 2 cm, (b) initial distance 2 cm but rounding an object. Dashes mark the daily measurements beginning at the second day. (c) Simulations for (a). Solid curves: glucose, dashed curve: tip density, both over the symmetry axis of the experiment. Left hand side: model without influence of glucose on the split rate and velocity of tips. Right hand side: splitting and growing stops if glucose density drops below 0.5 g/liter.

agreement in that the growth of the colonies stops at the point where the colonies are about to touch each other.

7 Conclusion

We have developed a model for the morphology and growth of *Phytophthora plurivora* depending on the supply of glucose and based on the correlated random walk with delay in the growth of newly split tips. In the first part of the paper, we investigated running fronts corresponding to the spread of *Phytophthora* in, say, an infected root, assuming that there is no feedback concerning defense on the part of the host. Using arguments based upon the considerations in [35], it is indeed possible to find running fronts if we have uniform turning kernels. These results have been extended to non-uniform kernels, using the Krein-Rutman theorem. While the role of the delay in the growth of new tips is unclear, the analysis shows that this delay affects the velocity of the front only weakly, but is essentially in forming the slope of the interface of the front: as growing hyphae only seldom change the direction, the front tends to be very, very steep. With respect to the application, especially the influence of the delay on different parameters of the front is of interest: we find that the observed delay in branching behavior has only a minor influence on the velocity resp. hyphal length, but a strong influence on the slope of the front. This finding can be understood intuitively, as the new tips only contribute to the generation of biomass in a delayed way, and this is not at the very edge of the front. Thus, the front is less steep and therefore the efficiency of the front-tips to spread and to find new regions well-supported with nutrient is not decreased by inter-tip competition. Especially if a region with low nutrient concentration is traversed, a steep front would decrease the ability of *Phytophthora* to find its way through this region into a zone with better food supply by unnecessary competition. The delay is able to prevent this undesired behavior. The theoretical dependence of the slope on velocity of the front, split rate, growth rate and delay can be nicely found in experimental data.

In the second part of our modeling approach is the interaction of tips concerning the spatial considerations. The density of hyphae of *Phytophthora* behind the interface is invariant so that growth happens at the front. This is, some factor prevents the tips to grow for ever. If this factor can be manipulated, this could lead to a way to control *Phytophthora*. Therefore, the model is augmented by the dynamics of glucose, and by a feedback of glucose depletion on the growth rate. Two kinds of experiments are used to validate and calibrate the model: the growth of one colony and the spatiotemporal distribution of the glucose concentration is monitored in a Petri dish. The second experiment is a confrontation experiment: two colonies growing in the same Petri dish. In the last experiment, the colonies stop to grow at the interface at the time point, when they almost touch respectively, the first hyphae meet but only when they grow in frontal manner. These experimental findings can be explained if we assume that the growth as well as the split rate tends to zero if the glucose rate drops below a critical level. No further interaction is required since resources are depleted. Based upon the parameters estimated as input, the model, augmented with the dynamics of glucose, has been simulated. Basically,

we find only a weak dependency on the glucose level but at a concentration between 0 and 1 g/L glucose, the growth- and the split rate breaks down. The velocity depicted in Fig. 4 is (at low glucose concentrations) only due to very few hyphae. The range of about 0.5 g/L glucose is in line with the experimental results that have been used to investigate the dependence of the model parameters on the glucose concentration (Fig. 4 and Fig. 5). A last observation shows that also the stop of growth in the center of a colony resp. behind the interface of a front could be explained in this way: the glucose data and simulations of a single colony (Fig. 8) shows that within a colony the glucose concentration is (after 3 days) below this critical value; only the edges of the front obtain enough glucose to be able to grow further or by any chance very few single hyphae may be able to grow further in order to search new sources of nutrient. In addition, the concentration of hyphae and tips behind the front may reach levels that do not allow a further growth.

All in all, we validated the model developed, checking the predicted slope of the front in dependence of the parameters measured versus the slope of the front obtained in the experiments. We find a satisfying agreement with experiments with *Phytophthora* performed in Petri dishes. The difference between data and model prediction can be easily explained by the simplicity of the turning kernels used in the theory.

The hope to reveal an intrinsic factor that stops *Phytophthora* to grow seems to fail if an susceptible host is however not able to activate any resistance mechanism or it is not successful: the only thing that stops *Phytophthora* is extreme starvation. And this will never happens in a living plant. The other way around we could hypothesize that the more aliments are available in the host tissue, the more efficient the pathogen will act as a sink via direct consumption of assimilates and increasing costs for repair and regrowth of damaged tissue. Hosts will be impaired by an enduring starvation and become susceptible to other stresses and pathogen attack.

References

1. M.D. Abramoff, P.J. Magelhaes and S.J. Ram. Image Processing with ImageJ, *Biophot. Internat.*, 11: 36–42, 2004.
2. H. Apel, M.S. Paudyal and O. Richter. Population dynamics and treatment strategies of *Phytophthora infestans* (late blight) in the Mid-Hills of Nepal, *Landschaftsökologie und Umweltforschung* 38: 1–12, 2002.
3. A.V. Brown and C.M. Brasier. Colonization of tree xylem by *Phytophthora ramorum*, *P. kernoviae* and other *Phytophthora* species. *Plant Pathol.* 56: 227–241, 2007.

4. D.M. Cahill, I.J. Bennett and J.A. McComb. Mechanisms of resistance to *Phytophthora cinnamomi* in clonal, micropropagated *Eucalyptus marginata*. *Plant Pathol.* 42: 865–872, 1993.

5. D.M. Cahill, J.E. Rookes, B.A. Wilson, L. Gibson and K.L. McDougall. *Phytophthora cinnamomi* and Australia's biodiversity: impacts, predictions and progress towards control, *Australian Journal of Botany*, 56: 279–310, 2008.

6. C. Clemenz, F. Fleischmann, K.-H. Häberle, R. Matyssek and W. Osswald. Photosynthetic and leaf water potential responses of *Alnus glutinosa* to stem-base inoculation with *Phytophthora alni subsp alni*, *Tree Physiology* 28: 1703-1711, 2008

7. E.A. Codling, M.J. Plank and S. Benhamou Random walk models in biology, *Journal of the Royal Society Interface* 5:813-834, 2008.

8. F.A. Davidson, B.D. Sleeman, A.D.M. Rayner, J.W. Crawford, and K. Ritz. Travelling waves and pattern formation in a model for fungal development. *J. Math. Biol.* 35: 589–608, 1997.

9. F.A. Davidson, G.P. Boswell, M.W.F. Fischer, L. Heaton, D. Hofstadler, M. Roper. Mathematical modelling of fungal growth and function. *IMAFungus* 2: 33–37, 2011.

10. D. Erwin and O. Ribeiro. *Phytophthora diseases world-wide*, APS Press, St. Paul MN, 1996

11. F. Fleischmann, S. Raidl and W.F. Osswald. Changes in susceptibility of beech (*Fagus sylvatica*) seedlings towards *Phytophthora citricola* under the influence of elevated atmospheric CO2 and nitrogen fertilization, *Environ. Poll.* 158: 1051-1060, 2010.

12. F. Fleischmann, A. Gottlein, H. Rodenkirchen, C. Lutz and W.F. Osswald. Biomass, nutrient and pigment content of beech (*Fagus sylvatica*) saplings infected with *Phytophthora citricola*, *P-cambivora*, *P-pseudosyringae* and *P-undulata*, *Forest Pathol.* 34: 79–92, 2004.

13. F. Fleischmann, J. Koehl, R. Portz, A.B. Beltrame and W.F. Osswald. Physiological change of *Fagus sylvatica* seedlings infected with *Phytophthora citricola* and the contribution of its elicitin "Citricolin" to pathogenesis, *Plant Biol.* 7: 650–658, 2005.

14. F. Fleischmann, D. Schneider, R. Matyssek and W.F. Osswald. Investigations on net CO_2 assimilation, transpiration and root growth of *Fagus sylvatica* infested with four different *Phytophthora* species, *Plant Biol.* 4: 144–152, 2002.

15. W.E. Fry, A.E. Apple and J.A. Bruhn. Evaluation of Potato Late Blight Forecasts Modified to Incorporate Host Resistance and Fungicide Weathering, *Phytopathology* 73(7): 1054–1059, 1983.

16. D.H. Griffin. *Fungal Physiology*, Wiley-Liss, Inc., 2nd edition, 1994.

17. K.P. Hadeler. Travelling fronts for correlated random walks, *Canadian Applied Math. Quart.* 2: 27–43, 1994.

18. K.P. Hadeler. Reaction transport systems. In: V. Capasso, O. Diekmann, Mathematics inspired by biology, 95-150, CIME Lectures 1997, Florence, *Lecture Notes in Mathematics* 1714, Springer Verlag 1999.

19. E.M. Hansen. Alien forest pathogens: *Phytophthora* species are changing world forests, *Boreal Environ. Res.* 13: 33–41 Suppl. A, 2008.

20. E.M. Hansen. A historical review of *Phytophthora* diseases, *Phytopathol.* 98: S196, 2008.

21. T.D. Harwood, X. Xub, M. Pautassoc, M.J. Jegerc and M.W. Shawa. Epidemiological risk assessment using linked network and grid based modelling: *Phytophthora ramorum* and *Phytophthora kernoviae* in the UK, *Ecol. Model.* 220: 3353–3361, 2009.

22. Th. Hillen and H.G. Othmer. The diffusion limit of transport equations derived from velocity-jump processes. *SIAM J. Appl. Math.*, 61: 751–775, 2001.

23. T. Jung and T.I. Burgess. Re-evaluation of *Phytophthora citricola* isolates from multiple woody hosts in Europe and North America reveals a new species, *Phytophthora plurivora sp nov.*, *Persoonia* 22: 95–110, 2009.

24. T. Jung. Beech decline in Central Europe driven by the interaction between *Phytophthora infections* and climatic extremes, *For. Path.* 39: 73–94, 2009.

25. P. Lax. *Functional Analysis*, Interscience Series in Pure and Applied Mathematics, Wiley, Chichester, 2002

26. T. Matsunaga, I. Karube and S. Suzuki. Some Observations on Immobilized Hydrogen-Producing Bacteria: Behavior of ydrogen in Gel Membranes, *Biotechnology and Bioengineering* 22:2607–2615, 1980.

27. A. Meskauskas, L.J. McNulty and D. Moore. Concerted regulation of all hyphal tips generates fungal fruit body structures: experiments with computer visualizations produced by a new mathematical model of hyphal growth. *Mycol. Res.* 108: 341–353, 2004.

28. M. Moslonka-Lefebvre, M. Pautasso, M.J. Jeger. Disease spread in small-size directed networks: Epidemic threshold, correlation between links to and from nodes, and clustering, *Journal of Theoretical Biology* 260: 402–411, 2009.

29. M.J. Plank and D.B. Sleeman. Lattice and non-lattice models of tumour angiogenesis, *Bull. Math. Biol.* 66, 1785-1819, 2004.

30. M.L. Ndeffo Mbah and Ch.A. Gilligan. Optimization of control strategies for epidemics in heterogeneous populations with symmetric and asymmetric transmission, *J. Theor. Biol.* 262: 757–763, 2010.

31. M. van Oijen. Selection and use of a mathematical model to evaluate components of resistance to *Phytophthora infestans* in potato, *Neth. J. Pl. Path.* 98: 192–202, 1992.

32. H.G. Othmer and A. Stevens. Aggregation, blowup and collapse: the ABC's of taxis and reinforced random walks. *SIAM J. Appl. Math.* 57, 1044-1081, 1997.

33. A. Pinzón, E. Barreto, A. Bernal, L. Achenie, A.F.G. Barrios, R. Isea and S. Restrepo. Computational models in plant-pathogen interactions: the case of *Phytophthora infestans*, *Theor. Biol. Med. Model.* 6: 24, 2009.

34. R.L. Portz, F. Fleischmann, J. Koehl, J. Fromm, D. Ernst, S.F. Pascholati and W.F. Osswald. Histological, physiological and molecular investigations of *Fagus sylvatica* seedlings infected with *Phytophthora citricola*, *Forest Pathol.* (in print) doi: 10.1111/j.1439-0329.2010.00667.x.

35. H.R. Schwetlick. Travelling fronts for multidimensional nonlinear transport equations, *Ann. Inst. Henri Poincaré, Analyse non linéaire* 17: 523–550, 2000.

36. H.R. Schwetlick. Uniqueness of travelling fronts for bistable nonlinear transport equations, *Bath Institute for Complex Systems*, Preprint 13/05, 2005.

37. P. Skelsey, G.J.T. Kessel, W.A.H. Rossing and W. van der Werf. Parameterization and Evaluation of a Spatiotemporal Model of the Potato Late Blight Pathosystem, *Analyt. Theor. Plant Pathol.*, 99: 290–300, 2009.

38. J.H. Smith. On the early groth rate of the individual fungus hypha, *New Pathologist* 24: 65–78, 1924.

39. P. Spanu and J. Kämper. Genomics of biotrophy in fungi and oomycetes – emerging patterns, *Curr. Opin. Plant Biol.* 13:409–414, 2010.

40. F.M. Thomas, R. Blank, G. Hartmann. Abiotic and biotic factors and their interactions as causes of oak decline in Central Europe, *For. Path.* 32: 277-307, 2002.

41. M. Thines and S. Kamoun. Oomycete–plant coevolution: recent advances and future prospects, *Curr. Opin. Plant Biol.* 13:427–433, 2010.

42. Th. Walther, H. Reinsch, K. Ostermann, A. Deutsch and Th. Bley. Applying dimorphic yeasts as model organisms to study mycelial growth: part 2. Use of mathematical simulations to identify different construction principles in yeast colonies. *Bioprocess Biosyst. Eng.* 34: 21–31, 2011.

43. J.E. Weiland, A.H. Nelson, G.W. Hudler. Aggressiveness of *Phytophthora cactorum*, *P. citricola I*, and *P. plurivora* from European Beech, *Plant Disease* 94: 1009-1014, 2010.

44. E. Zeidler. *Nonlinear Functional Analysis and its Applications I (Fixed-Points Theorems)*, Springer, Berlin etc., 1993.